Deformation and reconstruction mechanisms in coarse-grained superplastic Al-Mg alloys

Soer, W. A.; Chezan, A. R.; De Hosson, J. Th. M.

Published in:
Acta Materialia

DOI:
10.1016/j.actamat.2006.04.014

Publication date:
2006

Available online at www.sciencedirect.com
SCIENCE DIRECT
Acta Materialia 54 (2006) 3827–3833
Acta MATERIALIA
www.actamat-journals.com

Deformation and reconstruction mechanisms in coarse-grained superplastic Al–Mg alloys

W.A. Soer, A.R. Chezan, J.Th.M. De Hosson *

Department of Applied Physics, Materials Science Center and the Netherlands Institute for Metals Research, University of Groningen, Nijenborgh 4, 9747 AG Groningen, The Netherlands

Received 26 December 2005; received in revised form 2 April 2006; accepted 4 April 2006
Available online 27 June 2006

Abstract

This paper concentrates on the superplastic response of fine-grained and coarse-grained Al–Mg alloys under uniaxial tension. To identify the main characteristics of superplastic deformation and to determine the optimum deformation parameters, the microstructure and dislocation substructure of the alloys are analyzed as a function of strain, strain rate and temperature using electron backscatter diffraction and transmission electron microscopy (TEM). Under optimum deformation conditions of temperature and strain rate, these Al–Mg alloys have an elongation to failure in excess of 300%. Dynamic recrystallization is dominant at strain rates in excess of 10^{-1} s^{-1} and results in a strong coarsening of the microstructure and premature failure. Dynamic recovery prevails at a strain rate of around 10^{-2} s^{-1}, leading to great enhancement of the plasticity of the coarse-grained materials. TEM observations show that subgrain formation proceeds slowly. During initial straining, subgrains are formed primarily along the original grain boundaries. This results in a ''core and mantle'' microstructure, with dynamic recovery mainly taking place in the mantle region. A uniform substructure is established at a strain of the order of 1.

Keywords: Aluminum alloys; Superplasticity; Dynamic recrystallization; Transmission electron microscopy

1. Introduction

Conventional fine-grained superplasticity in Al–Mg alloys is based on grain boundary sliding as the primary deformation mechanism, which requires a fine, stable grain size of the order of 10 μm [1–4]. The main limitation towards mass application of these alloys is the relatively long forming time associated with a strain rate that is generally lower than 10^{-3} s^{-1}. The low strain rate is inherent to the diffusion-controlled mechanisms (e.g. dislocation climb) that accommodate grain boundary sliding [5]. The deformation at these strain rates is characterized by a high value of the strain rate sensitivity of the order of 0.5.

A reduction of the forming time by one or even more orders of magnitude can be obtained by using coarse-grained superplastic Al–Mg alloys, which present high ductility at strain rates of the order of 10^{-2} s^{-1} or higher [6–8]. It should be noted that since the mechanism of coarse-grained superplasticity does not follow the definition of superplasticity in the strictest sense, the deformation behavior has also been referred to as ''enhanced ductility'' or ''quasi-superplasticity'' by some researchers [9–11]. In this paper, we will maintain the designation ''coarse-grained superplasticity'' because of the low flow stress and relatively high strain rate sensitivity associated with this regime, both of which are characteristic of superplastic deformation.

The plastic deformation at high temperature of coarse-grained alloys is a complex phenomenon as grain size independent and grain size dependent mechanisms take place simultaneously [12]. Dynamic reconstruction in coarse-grained Al–Mg alloys is often evidenced by extensive grain refinement, which is attributed to the formation of subgrain boundaries and their conversion into low-angle and high-angle grain boundaries. This evolution of

* Corresponding author.
E-mail address: j.t.m.de.hosson@rug.nl (J.Th.M. De Hosson).

1359-6454/$30.00
doi:10.1016/j.actamat.2006.04.014

the microstructure in the solute-drag regime has been studied in detail in torsion [13] and compression [14] modes, but less in tension.

However, significant differences compared to these modes may arise in tensile deformation due to the anisotropy of the stress and the effect of strain localizations. Therefore in this study we concentrate on the superplastic response of fine-grained and coarse-grained Al–Mg alloys under uniaxial tension. To identify the main characteristics of superplastic deformation and to determine the optimum deformation parameters, the microstructure and dislocation substructure of the coarse-grained alloys are analyzed as a function of strain, strain rate and temperature using electron backscatter diffraction (EBSD) and transmission electron microscopy (TEM). The results are discussed in relation to the dynamic reconstruction mechanisms and their influence on the ductility of the alloys.

2. Experimental

The alloys used in this study are two coarse-grained Al–4.4% Mg and Al–4.4% Mg–0.4% Cu alloys with minor additions of Ti, Mn and Cr (<0.1%) and an average initial grain size of 70 μm, and a fine-grained Al–4.7% Mg–0.7% Mn alloy (AA5083) with an average grain size of 10 μm.

Specimens for tensile testing were laser cut from 2 mm thick cold-rolled metal sheets with the gauge direction parallel to the rolling direction and subsequently annealed for 10 min at 450 °C before deformation. Tensile elongation measurements were performed at constant crosshead speed under controlled temperature conditions using an Instron tensile machine and a three-zone-split furnace. The strain rate sensitivity index m and the activation energy Q were determined from strain rate change (SRC) experiments. The activation energy was calculated using the method described in Ref. [15]. The strain distributions over the gauge length were determined from optical measurements of the cross-sectional area of the gauge of the deformed specimens.

To investigate the microstructure during deformation, the tensile tests were interrupted by water quenching at several elongations up to 170%. The specimen surfaces were prepared for EBSD by electrochemical polishing in a 5% perchloric acid solution in methanol at −20 °C and 10 V. TEM specimens were laser cut from the gauges and thinned by twin-jet electrochemical polishing using the same electrolyte at −30 °C and 20 V.

3. Results and discussion

3.1. Macroscopic mechanical behavior and viscous dislocation glide

The dependence of the elongation to failure on strain rate and temperature for the two coarse-grained materials is presented in Fig. 1. Both alloys show maximum elongation to failure at a temperature between 400 and 440 °C,

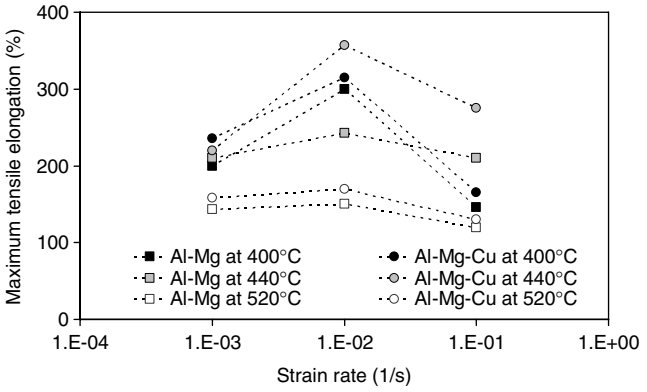

Fig. 1. Maximum elongation to failure as a function of strain rate at two different temperatures for the two coarse-grained Al–Mg alloys. Each data point represents the maximum out of three tensile tests.

which is considerably lower than the temperatures higher than 500 °C usually required to achieve maximum ductility in fine-grained Al–Mg alloys [16–18]. Furthermore, the optimum strain rate lies around 10^{-2} s^{-1}, which is high compared to the strain rates generally associated with the proposed grain boundary sliding mechanism in fine-grained materials. The fine-grained Al–Mg–Mn alloy (results not shown in Fig. 1) always yielded lower values for the maximum strain than the coarse-grained alloys when deformed under the same conditions of temperature and strain rate. Of the coarse-grained alloys, the Al–Mg–Cu showed on average slightly higher ductility than the Al–Mg alloy, the highest value for the tensile elongation being 357% for deformation at 440 °C at a strain rate of 10^{-2} s^{-1}. The relationship between flow stress and strain rate at several deformation temperatures for the coarse-grained Al–Mg–Cu and the fine-grained Al–Mg–Mn alloy is shown in Fig. 2. The data for the coarse-grained Al–Mg alloy follow exactly the same pattern as those for the Al–Mg–Cu alloy and have therefore been omitted. For the coarse-grained alloys, the $\log \sigma$ vs. $\log \dot{\varepsilon}$ dependence is linear over the entire strain rate interval investigated, while for the fine-grained Al–Mg–Mn alloy the dependence resembles the well-known sigmoidal shape [15].

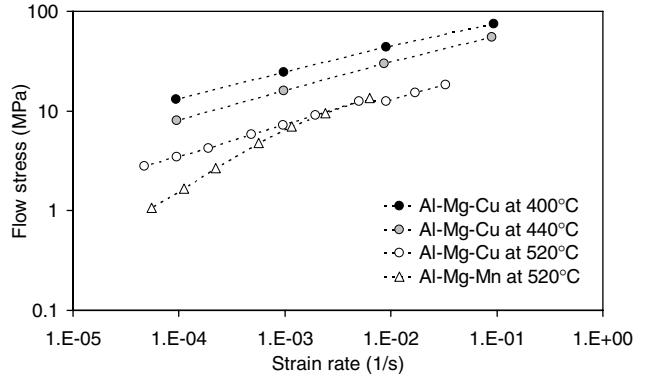

Fig. 2. Temperature dependence of the flow stress vs. strain rate relationship for the three aluminum alloys.

The strain rate sensitivity obtained from the data from Fig. 2 is plotted as a function of $\log \dot{\varepsilon}$ in Fig. 3. The fine-grained material deformed at 520 °C shows a peak for the strain rate sensitivity of about 0.7 at 10^{-4} s^{-1}, decreasing to a value of around 0.3 at 10^{-2} s^{-1}. The coarse-grained alloys are characterized by a relatively constant value for m of about 0.3. At a stress value of 25 MPa, the activation energy Q for the deformation of these alloys is equal to 153 kJ mol^{-1}, which is close to the activation energy for diffusion of Mg in Al (136 kJ mol^{-1}) [19] and the activation energy of self-diffusion (143 kJ mol^{-1}).

The values of the strain rate sensitivity index and the activation energy suggest that solute drag on dislocation gliding is the rate-controlling mechanism in these coarse-grained alloys. Nevertheless, it is relevant to examine critically this mechanism for the present case. In a Newtonian viscous material the component of the shear force $\tau_d b$ acting in the direction of the moving dislocation becomes equal to $B\bar{v}_d$ with $\bar{v}_d$ the mean velocity of the dislocations. The drag coefficient B consists of contributions from phonon viscosity, electron viscosity and impurity effects, but in the present case the drag term B is dominated by the impurity contribution (the electronic contribution is about 1 μPa s and the phonon contribution is even one order of magnitude smaller at 700 K), which may be written as [20]

$$B_{\mathrm{I,glide}} \simeq \frac{17}{4}\frac{A^2 c_0}{D_{\mathrm{Mg}} kT\Omega b} \tag{1}$$

where A is the elastic interaction energy term ($3\mu b\Omega\varepsilon_a/\pi$) and c_0 the concentration of Mg in Al. The drag coefficient can also be formulated depending on the dislocation velocity [21] but for the present case it gives similar values to those obtained through Eq. (1). Analogously, a different relation can be derived for the climb contribution to the drag term. Assuming that dislocation climb is not affected by the impurities and depends only on self-diffusion through the vacancy mechanism, we arrive at [22,23]

$$B_{\mathrm{I,climb}} = \frac{bkT}{2\pi D_{\mathrm{self}}\Omega}\ln\left(\frac{kTD_{\mathrm{self}}}{A\bar{v}_d}\right) \tag{2}$$

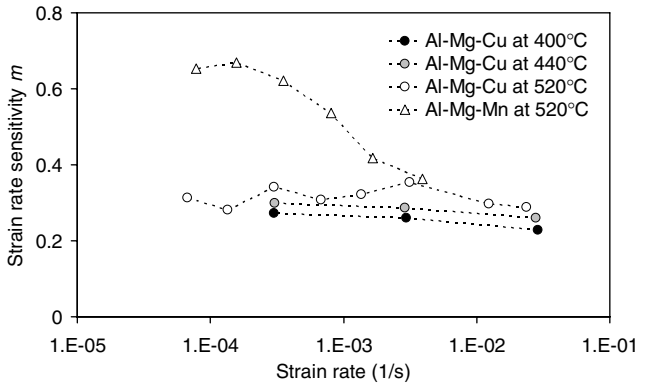

Fig. 3. Strain rate sensitivity (m) as a function of strain rate at different temperatures.

For solute drag on gliding dislocations to be the predominant mechanism, as is often claimed in the literature, $B_{\mathrm{I,glide}}$ should be considerably larger than $B_{\mathrm{I,climb}}$ because glide and climb are sequential steps in the deformation process and therefore the largest drag coefficient corresponds to the rate-determining mechanism. However, it should be realized that for the present case the condition $B_{\mathrm{I,glide}}/B_{\mathrm{I,climb}} \gg 1$ depends very critically on the precise value of the activation energy Q for diffusion of Mg in Al. Reported values for the activation energy range from 115 to 136 kJ mol^{-1} [19], depending on the experimental method used, leading to $B_{\mathrm{I,glide}}/B_{\mathrm{I,climb}} = 0.15$ and $B_{\mathrm{I,glide}}/B_{\mathrm{I,climb}} = 4.6$, respectively (both at 700 K). It should therefore be concluded that based on the reported values for the activation energies in the literature, both mechanisms may be active in the Al–Mg alloys at hand. The following gives further support to the solute drag mechanism.

As a matter of course the solute drag on gliding dislocations only operates if the solutes are able to interact with moving dislocations; no solute atmosphere will be formed if the dislocations are moving too fast. When the dislocation is moving with a velocity $\bar{v}_d$, an apparent flow relative to the dislocation has to be added to the flux equation [24–27] and beyond a critical value of the dislocation velocity $\bar{v}_c$, defined by

$$\bar{v}_c = \frac{3+2\sqrt{2}}{2}\frac{AD_{\mathrm{Mg}}}{b^2 k_B T} \tag{3}$$

the flow lines are open and do not pass through the dislocation core. The reason for a solute atmosphere being formed is that the flow lines of the Mg atoms end at the dislocation core. Therefore, a solute atmosphere can only be formed if the dislocation is moving more slowly than the critical velocity. In this case, the formation of a solute atmosphere leads to a concentration gradient and consequently a drag force per unit length can be defined. For $\bar{v}_d > \bar{v}_c$, the drag term $B_{\mathrm{I,glide}}$ is equal to zero. Note that D_{Mg} and thereby $\bar{v}_c$ depend strongly on temperature and activation energy. The critical velocity as a function of temperature has been calculated for the present case and it is displayed in Fig. 4. It can be concluded that if the dislocation velocity $\bar{v}_d$ is less than $5.\times10^{-4}$ m s^{-1} at $T = 700$ K, Mg solutes in Al can reach the core of moving dislocations and therefore solute drag on gliding dislocations can occur. The critical velocity poses an upper limit to the strain rates at which solute drag operates as given by the Orowan equation. For the strain rates used in this study (around 10^{-2} s^{-1}), a maximum dislocation velocity of $5.\times10^{-4}$ m s^{-1} requires a minimum mobile dislocation density of the order of 10^{11} m^{-2}. This value is substantially lower than the total dislocation densities typically encountered (larger than 10^{14} m^{-2}) and therefore it is concluded that solute atmospheres are formed at these strain rates.

The question may arise as to whether in superplastic deformation at high strain rates the plasticity-induced vacancy concentration becomes of the same order as the thermal vacancy concentration. From our earlier work

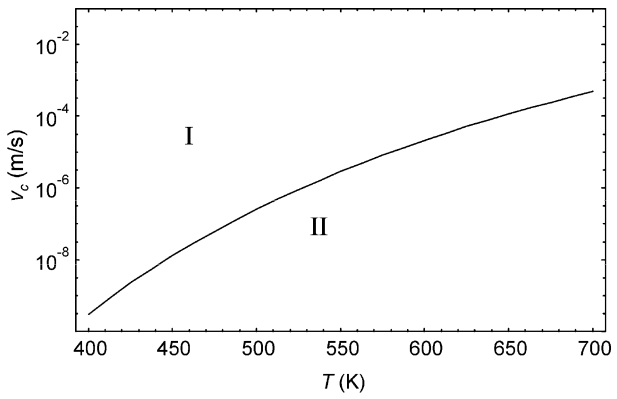

Fig. 4. Critical dislocation velocity for the formation of a solute atmosphere in Al–Mg as a function of temperature according to Eq. (3). In region I, the Mg solutes cannot reach the dislocation core and hence no solute atmosphere is created. In region II, the flow lines pass through the core and consequently solute drag takes place.

[28–30] it can be concluded that for this system the thermal vacancies are still dominant above 500 K. Since the superplastic temperature range for the coarse-grained Al–Mg alloys lies around 700 K, plasticity-induced vacancies are not expected to play a significant role in the climb and diffusional processes.

The strain rate sensitivity of the solute-drag mechanism is high enough to stabilize the plastic flow to such an extent that elongations of a few hundred per cent can be attained. However, although the solute drag operates relatively constantly throughout the entire range of strain rates investigated, the maximum elongation changes appreciably as a function of the strain rate as illustrated in Fig. 1. This shows that in addition to solute-drag creep, strain rate dependent reconstruction mechanisms greatly affect the ductility of the alloys.

3.2. Reconstruction mechanisms

The strain distribution over the gauge of two specimens, one fine-grained (Al–Mg–Mn) and one coarse-grained (Al–Mg–Cu), having the same value for the maximum tensile elongation (320%) is presented in Fig. 5. For both materials, the strain varies over the length of the gauge. In the case of the fine-grained material, about 5% of the gauge is heavily affected by cavitation [31,32]. The coarse-grained alloy shows prolonged necking over about 20% of the deformed gauge.

Because of the localization of strain, the strain rate in the necked region becomes much higher than the macroscopic strain rate of $10^{-2}\,s^{-1}$. This leads to the appearance of dynamic recrystallization close to the fracture place, as shown in Fig. 6(a). Dynamic recrystallization is presumably triggered by the high local dislocation densities generated at strain rates in excess of $10^{-1}\,s^{-1}$. The mechanisms involved in its nucleation and propagation cannot be conclusively identified from the present results; in particular, the mechanisms of oriented nucleation versus selective growth are widely debated in the literature [33]. Oriented

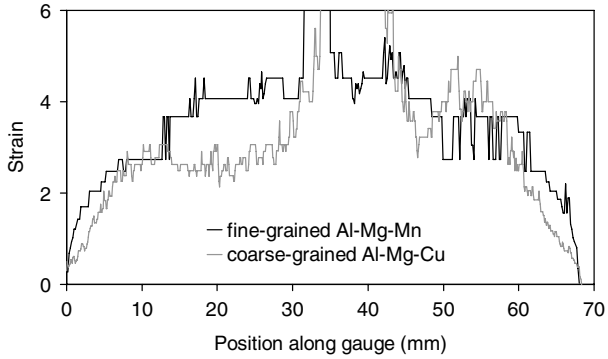

Fig. 5. Strain distribution over the gauge length of two deformed specimens. The fine-grained Al–Mg–Mn alloy was deformed 320% at 520 °C and $10^{-3}\,s^{-1}$ and the coarse-grained Al–Mg–Cu was deformed 320% at 420 °C and $10^{-2}\,s^{-1}$.

nucleation is often observed in the presence of second-phase particles. This so-called particle-stimulated nucleation is evidently not relevant in our coarse-grained alloys. Reports of texture development during dynamic recrystallization indicate that selective growth plays a significant role in face-centered cubic metals [34]. The texture observed in the recrystallized parts of the Al–Mg specimens is similar to that of the uniformly deformed gauge, suggesting that selective growth may indeed be responsible for the microstructure observed. The new grains coarsen rapidly, producing inhomogeneities of the microstructure and consequently a premature failure of the material. It should be noted that irregularities in the material lead to necking in the first place; however, large grains of the size shown in Fig. 6(a) were not found in the material prior to deformation and their development is therefore positively attributed to dynamic recrystallization.

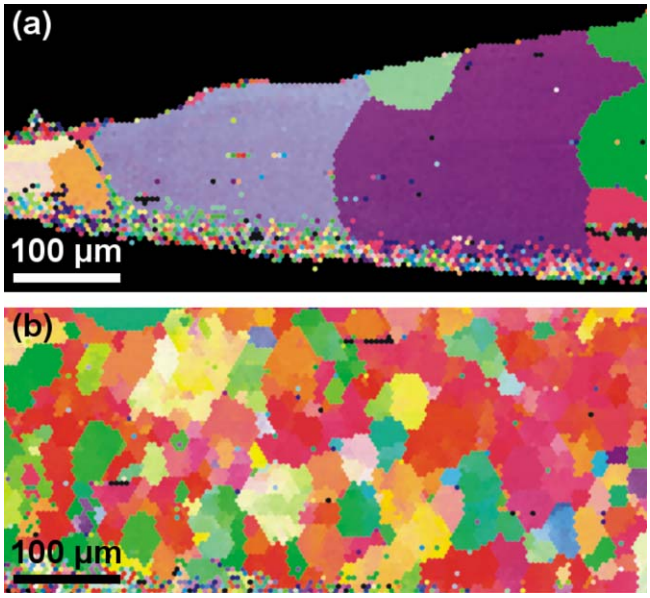

Fig. 6. Grain structure of the coarse-grained Al–Mg–Cu alloy deformed 320% at 420 °C and $10^{-2}\,s^{-1}$ (a) close to the fracture area and (b) in the uniformly deformed gauge.

Table 1
Average grain size of Al–Mg–Cu alloy before deformation and as deformed at various strain rates and temperatures

Temperature (°C)	Strain rate (s^{-1})	Average grain size (μm)
Before deformation		115
420	10^{-3}	64
420	10^{-2}	43
420	10^{-1}	95
450	10^{-1}	171

The grain sizes are measured from EBSD scans, requiring a misorientation of at least 5° in order for a grain to be counted.

At intermediate strain rates ($10^{-2}\ s^{-1}$), the main restoration mechanism in the coarse-grained alloys is dynamic recovery. This mechanism is associated with annihilation of dislocations and with the formation of a subgrain structure [12]. The newly generated microstructure, as illustrated in Fig. 6(b), is characterized by a finer grain size and an increased grain boundary density as compared to the original material. The grain refinement is a result of the continuous increase in subgrain boundary misorientations so that they become typical of low-angle and in some cases even high-angle grain boundaries. Analysis of the misorientation angles shows a significant increase of the ratio of low-angle to high-angle boundaries in this regime [8]. The dynamic recovery greatly improves the ductility of the coarse-grained materials leading to values of the maximum strain in excess of 300%.

A quantitative measure of dynamic recovery is provided by the extent of grain refinement as measured by EBSD. Table 1 shows the average grain size of the coarse-grained alloy deformed to failure at different strain rates and temperatures compared to the original grain size. The maximum grain refinement at a deformation temperature of 420 °C is attained at a strain rate of about $10^{-2}\ s^{-1}$. At lower strain rates, the formation of a subgrain structure is suppressed, while at higher strain rates or temperatures, dynamic recrystallization becomes predominant and leads to rapid grain growth. A similar trend is shown by the evolution of texture during deformation as shown in Fig. 7. The cube texture that develops along the tensile axis becomes most pronounced at the optimum strain rate of $10^{-2}\ s^{-1}$. The evolution of this texture is associated with the formation of a substructure during dynamic recovery, allowing favorable orientations of the subgrains with respect to the tensile axis. In tensile deformation of fine-grained Al–Mg [35], it was found that at a strain rate of $10^{-4}\ s^{-1}$, when grain boundary sliding dominates, the texture is significantly reduced; at a strain rate of $10^{-2}\ s^{-1}$, when solute-drag creep is the rate-controlling mechanism, a strong cube texture developed similar to our observations.

3.3. Dislocation substructure

Fig. 8 shows three micrographs representative of the microstructural evolution observed during superplastic forming of the coarse-grained Al–Mg alloy. At a strain of a few per cent, just beyond the yield point, random configurations of dislocations are visible (Fig. 8(a)). This stage of deformation is characterized by a drop of the flow stress [8], which indicates dislocation multiplication from an initially low dislocation density pinned by Mg solutes [36]. During further straining, subgrain formation occurs primarily along the original grain boundaries, as in Fig. 8(b) showing subgrain boundaries near a high-angle boundary triple junction. At this stage, the substructure shows many incomplete subgrain boundaries, i.e. boundaries with a very low misorientation (<1°) that do not fully enclose a subgrain. Only when a strain of the order of 1 is attained do the subgrains completely fill the grain interior. Fig. 8(c) shows the refined subgrain structure at a strain of 170% and an average subgrain size of approximately 5 μm. Note that the size distribution is fairly broad, with observed subgrain sizes ranging from 1 to 10 μm. The subgrain boundaries have an average misorientation of the order of 2°, with some of the boundaries having misorientations high enough to be detected by EBSD. Essentially the same substructure evolution was found in the Al–Mg–Cu alloy.

Without any external stress applied, the subgrain boundaries are relatively stable under annealing at superplastic forming temperature as illustrated in Fig. 9. At this temperature, most of the lattice dislocations are absorbed into the subgrain boundaries, and some rearrangement of the dislocations in the subgrain boundaries is observed. However, the subgrain structure as a whole remains intact

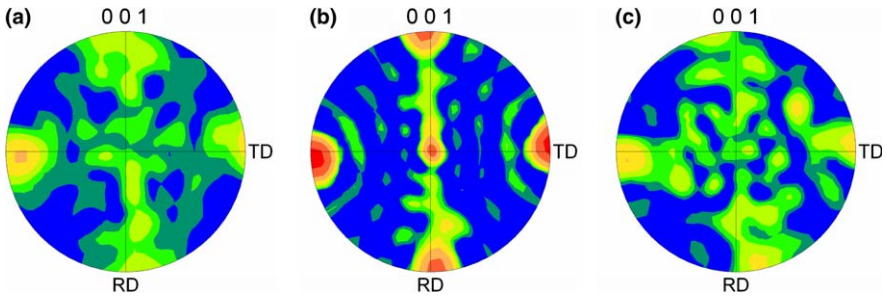

Fig. 7. (001) pole figures for the Al–Mg–Cu alloy deformed at 420 °C at (a) $10^{-3}\ s^{-1}$, (b) $10^{-2}\ s^{-1}$ and (c) $10^{-1}\ s^{-1}$. Dynamic recovery leads to a pronounced cube texture at a strain rate of $10^{-2}\ s^{-1}$.

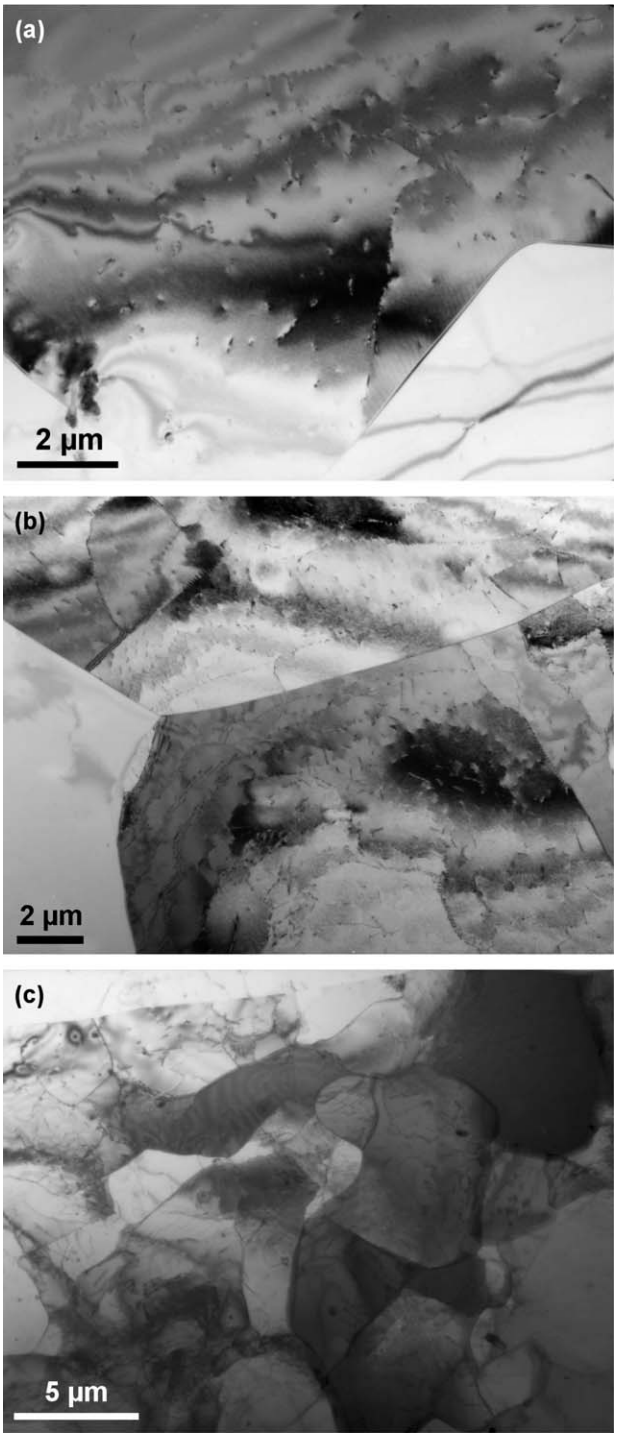

Fig. 8. Dislocation substructure in Al–Mg deformed at 440 °C and $5. \times 10^{-3}\ s^{-1}$ to (a) 4%, (b) 20% and (c) 170%.

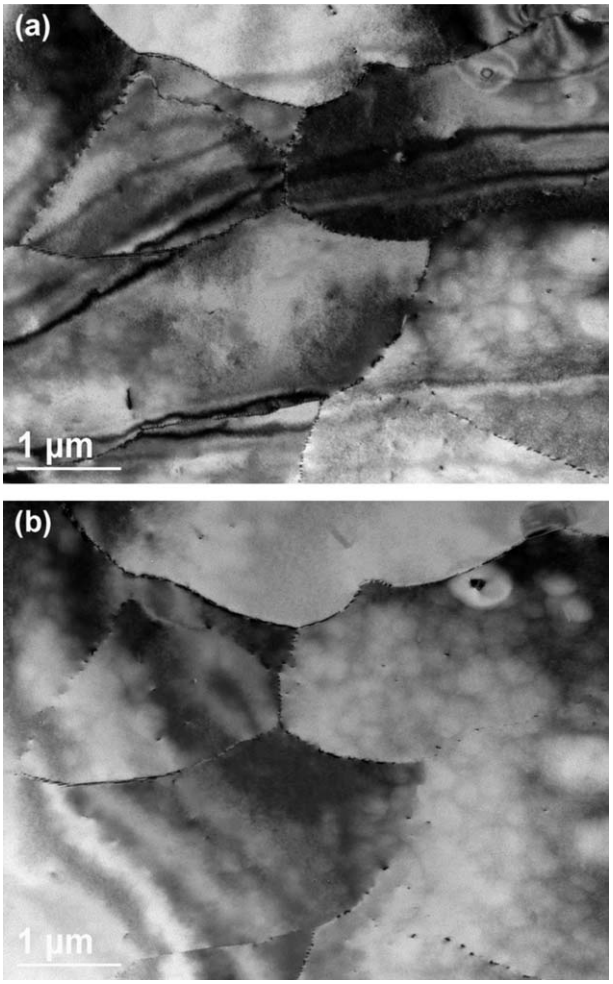

Fig. 9. Subgrains in Al–Mg–Cu (a) at room temperature and (b) after in situ annealing at 450 °C for 10 min.

for at least 10 min, even in a thin TEM foil, where dislocations can easily escape to the free surfaces of the specimen. Given the strain rate around $10^{-2}\ s^{-1}$, this is a long enough time to ensure that the observed recovery mechanisms are dynamic rather than static.

Our observations of subgrain formation are similar to those of binary Al–Mg alloys in torsion [13] and compression [14] in the solute-drag regime. However, since the maximum achievable strain in tensile mode is considerably lower, the grains do not thin to such an extent that so-called geometric dynamic recrystallization [37] becomes relevant. In all deformation modes, the substructure formation in the Al–Mg alloys is more sluggish than in pure Al, presumably due to a lowering of the stacking fault energy by the solute Mg [38].

The effect of the Mg content on the tensile ductility is twofold. On the one hand, a higher Mg content increases the extent of solute drag, thereby stabilizing the plastic flow. However, beyond a few per cent Mg, the effect on the strain rate sensitivity becomes fairly marginal; Taleff et al. [10] reported an increase of $m = 0.29$–0.32 in going from 2.8% to 5.5% Mg. On the other hand, the presence of Mg significantly reduces dynamic recovery as evidenced by the slow formation of subgrains. As a result, Mg concentrations above 5% can easily give rise to dynamic recrystallization within a certain domain of temperature and strain rate, which in the absence of grain-refining second-phase particles leads to rapid coarsening of the microstructure. The currently used composition with 4.4% Mg appears to be a good balance between solute drag and

dynamic recovery, leading to enhanced tensile ductility in excess of 300%. In torsional deformation, where a high strain rate sensitivity to avoid necking is less important, the ductility benefits most from dynamic recovery (leading to geometric dynamic recrystallization at high strains) and is consequently higher for pure Al than for Al–Mg alloys [39].

The initially inhomogeneous formation of subgrains gives rise to a "core and mantle" microstructure, in which most deformation is concentrated along the grain boundaries. In fine-grained superplasticity, this type of microstructure has been associated with grain mantle deformation processes as an accommodating mechanism for grain boundary sliding [40]. In the present case, the concentration of dislocation structures in the mantle region is attributed to dynamic recovery and can be explained by the high stresses exerted by dislocation pile-ups at the grain boundaries, which promote dislocation climb and consequently dynamic recovery. The formation of subgrains and the continuous increase in subgrain boundary misorientation due to absorption of dislocations effectively lead to grain refinement near the original grain boundaries. The newly formed grains may subsequently accommodate deformation by a grain boundary sliding mechanism analogously to conventional fine-grained superplastic alloys and thus contribute significantly to the ductility of the coarse-grained alloys.

4. Conclusions

Under optimum deformation conditions of temperature and strain rate, coarse-grained Al–Mg alloys can have an elongation to failure in excess of 300%. Experimental and theoretical analyses show that the principal mechanism of plasticity in these alloys is solute drag on gliding dislocations but that a combined mechanism of dislocation climb cannot be fully excluded. The plasticity of these materials is strongly influenced by dynamic reconstruction mechanisms. Dynamic recrystallization is dominant at strain rates in excess of $10^{-1}\,s^{-1}$ and results in a strong coarsening of the microstructure and premature failure. Dynamic recovery prevails at a strain rate around $10^{-2}\,s^{-1}$, leading to great enhancement of the plasticity of the coarse-grained materials.

During dynamic recovery, grain refinement occurs by the formation of subgrain boundaries and low-angle grain boundaries. TEM observations show that subgrain formation proceeds slowly, presumably due to a relatively low stacking fault energy combined with a low density of second-phase particles. During initial straining, subgrains are formed primarily along the original grain boundaries. This results in a "core and mantle" microstructure, with dynamic recovery mainly taking place in the mantle region. A uniform substructure is established at a strain of the order of 1.

Acknowledgement

This work was funded by the Netherlands Institute for Metals Research under project numbers MC4.01104 and MC4.02128.

References

[1] Edington JW. Metall Trans A 1982;13:703.
[2] Hales SJ, McNelley TR. Acta Metall 1988;36:1229.
[3] Sherby OD, Wadsworth J. Prog Mater Sci 1989;33:169.
[4] Kulas MA, Green WP, Taleff EM, Krajewski PE, McNelley TR. Metall Mater Trans A 2005;36:1249.
[5] Kassner ME, Pérez-Prado MT. Prog Mater Sci 2000;45:1.
[6] Yoshida H, Tanaka H, Takiguchi K. European Patent 0846781.
[7] Kim WJ. Mater Sci Forum 1999;304–306:273.
[8] Chezan AR, De Hosson JTM. Mater Sci Forum 2005;495–497:883.
[9] Taleff EM, Lesuer ER, Wadsworth J. Metall Mater Trans A 1996;27:343.
[10] Taleff EM, Henshall GA, Nieh TG, Lesuer DR, Wadsworth J. Metall Mater Trans A 1998;29:1081.
[11] Woo SS, Kim YR, Shin DH, Kim WJ. Scripta Mater 1997;37:1351.
[12] McQueen HJ, Evangelista E, Kassner ME. Z Metallkd 1991;82:336.
[13] Henshall GA, Kassner ME, McQueen HJ. Metall Trans A 1992;23:881.
[14] Drury MR, Humphreys FJ. Acta Metall 1986;34:2259.
[15] Bae DH, Ghosh AK. Acta Mater 2000;48:1207.
[16] Li F, Roberts WT, Bate PS. Acta Mater 1996;44:217.
[17] Nieh TG, Hsiung LM, Wadsworth J, Kaibyshev R. Acta Mater 1998;46:2789.
[18] Kaibyshev R, Musin F, Lesuer DR, Nieh TG. Mater Sci Eng A 2003;342:169.
[19] Sherby OD, Taleff EM. Mater Sci Eng A 2002;322:89.
[20] Cottrell AH, Jaswon MA. Proc R Soc Lond A 1949;199:104.
[21] Mohamed FA, Langdon TG. Acta Metall 1974;22:779.
[22] Hirth JP, Lothe J. Theory of dislocations. New York (NY): John Wiley; 1968.
[23] Takeuchi A, Argon AS. Acta Metall 1976;24:883.
[24] Eshelby JD. Proc Roy Soc A 1949;62:307.
[25] Weertman J, Weertman JR. In: Nabarro FRN, editor. Dislocations in solids, vol. 3. Amsterdam: North-Holland; 1980 [chapter 8].
[26] Hirth JP, Zbib HM, Lothe J. Model Simul Mater Sci Eng 1998;6:165.
[27] Yoshinaga H, Toma K, Abe K, Morozumi S. Philos Mag 1971;23:1387.
[28] Detemple K, Kanert O, Murty KL, De Hosson JTM. Phys Rev B 1991;44:1988.
[29] Detemple K, Kanert O, De Hosson JTM, Murty KL. Phys Rev B 1995;52:125.
[30] Michael K, Kanert O, Kuchler R, De Hosson JTM. Solid State Commun 2004;129:727.
[31] Pilling J, Ridley N. Res Mech 1988;23:31.
[32] Bae DH, Ghosh AK. Acta Mater 2002;50:993;
Bae DH, Ghosh AK. Acta Mater 2002;50:1011.
[33] Doherty RD, Hughes DA, Humphreys FJ, Jonas JJ, Juul Jensen D, Kassner ME, et al. Mater Sci Eng A 1997;238:219.
[34] Tóth LS, Jonas JJ. Scripta Metall Mater 1993;27:359.
[35] Martin CF, Blandin JJ, Salvo L. Mater Sci Eng A 2000;297:212.
[36] Usui E, Inaba T, Shinano N. Z Metallkd 1986;77:179.
[37] McQueen HJ, Knustad O, Ryum N, Solberg JK. Scripta Metall 1985;19:73.
[38] Schlagowski U, Kanert O, De Hosson JTM, Boom G. Acta Metall 1988;36:865.
[39] Gourdet S, Montheillet F. Mater Sci Eng A 2000;283:274.
[40] Gifkins RC. Metall Trans A 1976;7:1225.